PUBLICATIONS OF THE ASTRONOMICAL SOCIETY OF THE PACIFIC, **122**:470–484, 2010 April

Thirty Meter Telescope Site Testing X: Precipitable Water Vapor

A. OTÁROLA,[1] T. TRAVOUILLON,[1] M. SCHÖCK,[2] S. ELS,[3,4] R. RIDDLE,[1] W. SKIDMORE,[1] R. DAHL,[5] D. NAYLOR,[5] AND R. QUEREL[5]

Received 2009 December 2; accepted 2010 January 30; published 2010 March 19

ABSTRACT. The results of the characterization of precipitable water vapor in the atmospheric column carried out in the context of identifying potential sites for the deployment of the Thirty Meter Telescope (TMT) are presented. Prior to starting the dedicated field campaign to look for a suitable site for the TMT, candidate sites were selected based on a climatology report utilizing satellite data that considered water vapor as one of the study variables. These candidate sites are all of tropical or subtropical location at geographic areas dominated by high-pressure systems. The results of the detailed on-site study, spanning a period of 4 yr, from early 2004 until the end of 2007, confirmed the global mean statistics provided in the previous reports based on satellite data, and also confirmed that all the candidate sites are exceptionally good for astronomy research. At the locations of these sites, the atmospheric conditions are such that the higher the elevation of the site, the drier it gets. However, the data analysis shows that during winter, San Pedro Mártir, a site about 230 m lower in elevation than Armazones, is drier than the Armazones site. This finding is attributed to the fact that Earth's atmosphere is largely unsaturated, leaving room for regional variability; it is useful in illustrating the relevance of in situ atmospheric studies for understanding the global and seasonal variability of potential sites for astronomy research. The results also show that winter and spring are the driest seasons at all of the tested sites, with Mauna Kea (in the northern hemisphere) and Tolonchar (in the southern hemisphere) being the tested sites with the lowest precipitable water vapor in the atmospheric column and the highest atmospheric transmission in the near and mid-infrared bands. This is the tenth article in a series discussing the TMT site-testing project.

1. INTRODUCTION

This article is part of series of papers reporting on the results of the TMT site-testing campaign. The site-testing effort was centered on a multiyear on-site study of the characteristics of five candidate sites and included the measurements of weather-related, turbulence-related and other atmospheric parameters of interest. The focus of this manuscript is the discussion of the results of the statistical characterization of water vapor in the atmospheric column at these sites. A complete description of the parameters of interest, the location and physical description of the candidate sites, and the suite of instruments used to study all these parameters of interest is included in the first paper of this series (Schöck et al. 2009).

The approach taken by TMT to pick the candidate sites from a larger list of potential sites for the project was based in part on remote sensing studies that, among other parameters, reported on the mean values of precipitable water vapor (PWV) at these sites. The aim of the TMT on-site testing campaign was to deploy instrumentation at five candidate sites, those listed in Table 1, to monitor the PWV in the atmospheric column through the years and gather enough data to compute the statistics from in situ observations. Unfortunately, some aspects related to the maturity of the radiometers used to monitor the PWV and the remoteness of the candidate sites resulted in a shorter than desired on-site data series. Therefore, for the three TMT candidate sites located in northern Chile (Tolar, Armazones, and Tolonchar), PWV is estimated from in situ surface water-vapor density together with a water-vapor scale height that was computed for the different seasons from atmospheric soundings obtained from the city of Antofagasta in northern Chile. For the 13N site at Mauna Kea (Hawaii), PWV was estimated from an existing database of time series of optical depths observed at 225 GHz, and for the San Pedro Mártir site (Baja California, Mexico), PWV was estimated from an existing database of optical depths at 210 GHz. Consequently, these additional databases, which consist of atmospheric transparency measurements at specific wavelengths that could be converted to equivalent PWV by means of radiative transfer models, atmospheric soundings from nearby stations, and in situ surface weather data, proved essential for confirmation of the validity of the overall statistics found by means of the preliminary remote sensing studies.

The reasons for monitoring PWV, the experience of TMT in the in situ monitoring of this variable, and the data sets used for

[1] TMT Observatory Corporation, Pasadena, CA 91107.
[2] TMT Observatory Corporation, Victoria, BC, Canada.
[3] Cerro Tololo Inter-American Observatory, La Serena, Chile.
[4] Gaia DPAC Project Office, ESAC, Madrid, Spain.
[5] Institute for Space Imaging Science, University of Lethbridge, Alberta, Canada.

TABLE 1
LIST OF TMT CANDIDATE SITES SELECTED FOR IN SITU TESTING AND THEIR COORDINATES

Site name	Elevation (m)	Latitude (deg)	Longitude (deg W)	PWV Median (mm)	PWV 10% (mm)
Cerro Tolar	2290	−21.9639	70.0997	4.02	1.59
Cerro Armazones	3064	−24.5800	70.1833	2.87	1.15
Cerro Tolonchar	4480	−23.9333	67.9750	1.70	0.70
San Pedro Mártir	2830	+31.0456	115.4691	2.63	1.06
Mauna Kea 13N	4050	+19.8330	155.4810	1.86	0.72

NOTE.—The median and best 10% percentile of PWV are estimated from the remote sensing studies. Specifically, the PWV was estimated from 6.7 μm thermal emission, originating mainly between the 300 hPa and 600 hPa pressure levels, detected by instruments onboard the GOES-8 satellite and making use of collocated temperature information from nearby radiosonde stations.

confirming the results from the preliminary remote sensing studies are described in this article.

1.1 The Relevance of Monitoring Water Vapor for TMT

Atmospheric water vapor is one of the main sources of opacity throughout the infrared spectral region, and the dominant source of opacity at mid and far-infrared wavelengths. The monitoring of PWV in the atmospheric column, ideally through several annual cycles, is thus one of the most relevant variables for the determination of the best location for the deployment of astronomical observatories with instrumentation in the microwave, millimeter, submillimeter and infrared bands (see, for instance, Giovanelli et al. 2001). Of particular importance for TMT, the atmospheric thermal background constitutes a large noise component on mid-infrared observations, the effect being so strong that any improvement in site quality translates directly into a significantly better sensitivity of astronomical observations (Chamberlain 2001).

Specifically, the TMT science objectives require a diffraction-limited large-aperture telescope capable of high-resolution spectroscopy and imaging in the near- and mid-infrared bands. From the point of view of mid-infrared observations, a high-altitude site with low PWV content in the atmospheric column is therefore favorable for TMT. The reduction in the width of the pressure-broadened atmospheric lines results in lower thermal background and greater atmospheric transparency.

1.2 General Aspects in the Global Distribution of Water Vapor

Figure 1 depicts, with a $1° \times 1°$ horizontal resolution, the monthly average global distribution of PWV from data gathered with the Atmospheric Infrared Sounder (AIRS, Aumann et al. 2003) sensor on board the NASA Aqua satellite.[6] For the interested reader, other global water vapor data sets with resolution of $1° \times 1°$ using data from various remote sensing sensors and radiosondes are described in Randel et al. (1996) and Simpson et al. (2001), respectively. Specifically, the data represented in Figure 1 correspond to the PWV monthly average of 2002 September and help illustrate the following aspects in the distribution of PWV: (a) the strong gradient with longitude with higher levels of water vapor in the Inter-Tropical Convergence Zone (ITCZ[7]) due to evaporation induced by the larger sensible heat flux from the Sun, and lower PWV levels in the polar regions; (b) the variation with geographic altitude is clearly inferred from the drier regions matching the location of high elevation mountain ranges such as the occidental side of the Americas, the southwest section of Africa and central Asia; and (c) the humid feature associated with the low-pressure system over the Amazon region, and the dry areas associated with the subsidence air of the high-pressure systems off the coast of northern Chile and the west coast of Australia, among others.

At a regional scale, the relative dryness of regions around the world are associated with a combination of factors including: geomorphology, geographical altitude, air temperature, regional circulation, and existence of subsidence temperature inversion layers. Specifically, temperature inversions help to trap the humidity below the cap of the inversion, preventing water vapor from mixing with higher levels in the atmosphere. Other factors could be low-level orographic circulations that induce lifting of the humid air mass reaching precipitation windward of mountains, with the net result of advection of dry air over the lee side of the mountains. Good examples include the combination of several of these factors that explains the dryness of the Atacama Desert region (Otárola et al. 1998); the combination of orographic precipitation, advection of dry air, and geographical altitude that explain the dryness of Mauna Kea; and water vapor concentrations limited by very cold temperatures, such as in the case of the Antarctic high plateau (see Fig. 1 in Minier et al. 2008).

[6] Extracted from http://disc.sci.gsfc.nasa.gov/AIRS/data-holdings/by-data-product/.

[7] ITCZ, the Inter-Tropical Converging Zone, centered mainly at about 5° north of the equator, is the latitude band over the Pacific and Atlantic oceans where the northern and southern hemisphere trade winds converge (Wallace & Hobb 2006; Takahashi & Battisti 2007).

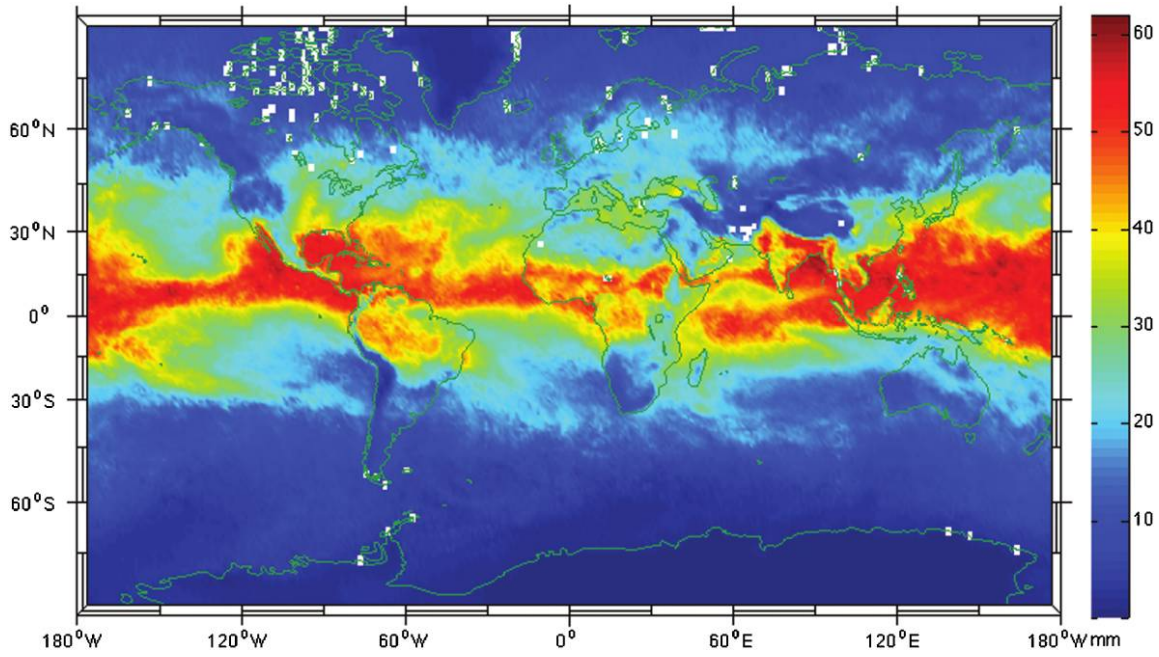

FIG. 1.—Example of the global distribution of monthly PWV, showing the global monthly average of PWV in 2002 September; it was done as part of this study using data obtained from the Atmospheric InfraRed Sounder (AIRS) database.

On a global scale, the water-vapor distribution retains seasonal characteristics. However, on a regional scale, changes in the regional circulation introduce significant variations in the absolute humidity levels. Good examples are the monsoon patterns affecting the northwest of Mexico and southwest of the US (Maddox et al. 1995; Adam & Comrie 1997, Kursinski et al. 2008) and east Asia (Lau & Li, 1984), as well as the advection of humid air from the Amazon basin over to the Atacama region that is associated with the southward shift and weakening of the high-pressure system off the coast of northern Chile (Fuenzalida et al. 1987; Zhou & Lau, 1998).

The coordinates and altitudes of the five sites tested by TMT are listed in Table 1; they are all tropical or subtropical locations in geographic areas that are dominated by high-pressure systems during a significant part of the year.

2. TMT SITE TESTING: PRELIMINARY STUDIES

Because of the high cost of instrumentation needed for accurate characterization of the transparency and stability of the atmosphere at potential sites for the deployment of astronomical facilities, and because of the expensive logistics that are required, it is advisable to begin with preliminary studies based on prior experience and with existing climate databases to establish the mean magnitude of the parameters that are relevant for the specific site-selection process. Consequently, the selection of the candidate sites for the Thirty Meter Telescope (TMT) is the result of accumulated knowledge, mostly obtained from earlier site-testing studies of geographical areas around the globe that have been found to meet the requirements for ground-based observatories, together with logistical considerations. This process limited the possible regions to northern Chile, the southwestern continental US, northern Mexico, and the Hawaiian Islands (Walker et al. 2002). In addition, three specific remote sensing studies, in the form of internal reports by Erasmus & van Staden (2001, 2002, 2003),[8] were undertaken for TMT and its precursor projects and partners. These studies provided information on cloud cover and PWV in northern Chile in the region bounded by latitudes 20.5° S to 30.5° S and longitudes 66° W to 72° W, and in the southwest US and northern Mexico over the area 18° N to 40° N and 96° W to 124° W (Erasmus 2005) and Mauna Kea.

Other large aperture projects, such as the European Extremely Large Telescope (E-ELT), have invested in putting together a worldwide climatology database that allows us to identify good candidate sites for the location of astronomical projects and keep track of possible trends in the relevant atmospheric variables of interest (Sarazin 2005).

Table 1 includes, for the five candidate sites, the median and best 10 percentile of PWV estimated from the remote sensing studies. Specifically, the PWV was estimated from 6.7 μm thermal emission, originating mainly between the 300 hPa and 600 hPa pressure levels, detected by instruments on board the *GOES-8* satellite and making use of collocated upper-troposphere

[8] There are plans to make these internal studies available in the open scientific literature.

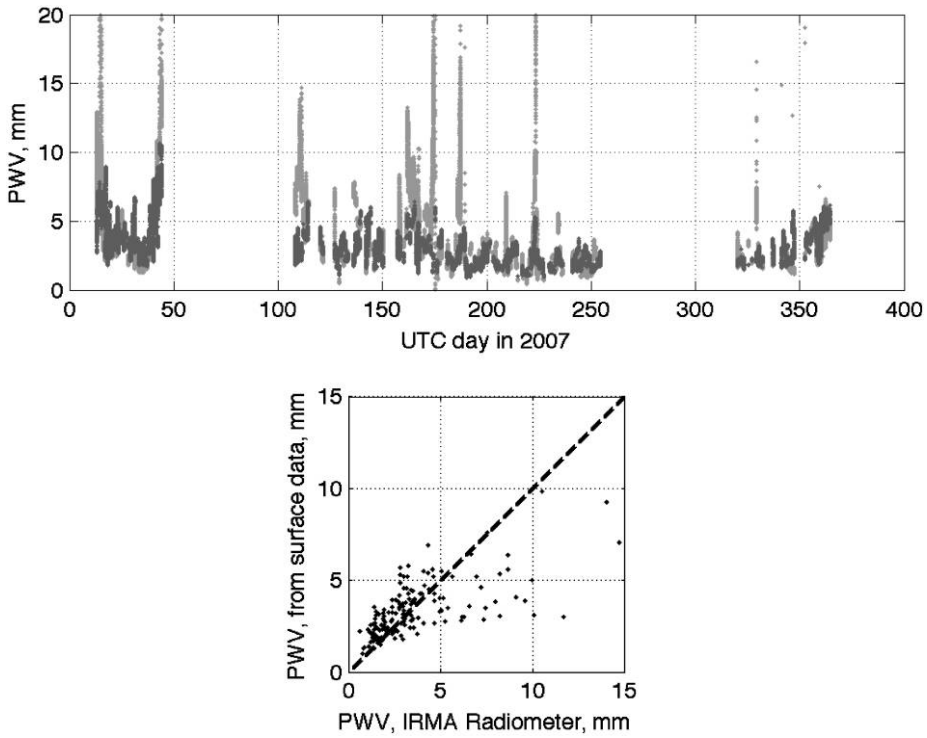

FIG. 2.—Armazones site: Comparison of collocated PWV data series obtained with the IRMA radiometers (*gray*) and that derived from measurements of the surface water vapor density (*black*). The water vapor scale heights used to estimate PWV from surface water vapor density are: 1.55 km for summer season data and 1.74 km for all of the other seasons (scale heights were obtained from the analysis of radiosonde profiles). See the electronic edition of the *PASP* for a color version of this figure.

temperature information from radiosondes launched from nearby sounding stations. For a detailed description of the methodology used to estimate PWV from 6.7 μm radiances, see Erasmus & Sarazin (2001, 2002).

These preliminary studies were followed by a site-testing campaign intended to provide a more complete understanding of the statistics and variability of all the parameters of interest, water vapor included. This article provides a more detailed description of the equipment used for the monitoring of precipitable water vapor in the atmospheric column (§§ 3 and 4), results (§ 5), as well as interpretation of results and conclusions (§§ 6 and 7).

3. INSTRUMENTS AND DATABASES USED FOR THE CHARACTERIZATION OF PWV AT THE TMT CANDIDATE SITES

This series of TMT site-testing papers is an effort not only to share with the scientific community the results of the site-testing campaign, but also to share the lessons learned in the process. Specifically, one lesson learned was that the maturity of the instruments used to monitor site characteristics is crucial for the success of the campaign. In the specific case of the radiometers intended to be used as the main source of integrated water vapor measurements, additional effort was required to improve their calibration and reliability, which resulted in a more limited data set than originally desired. However, in the end, the validity of the measurements taken could be shown and the data set was used to validate other PWV data series, such as those estimated from surface water vapor density computed from in situ measurements of temperature and relative humidity.

3.1 The IRMA Infrared Water Vapor Radiometers

For the monitoring of the integrated water vapor in the atmospheric column above the candidate sites, the TMT project decided to use three Infrared Radiometers for Millimetre Astronomy (IRMA), built by the University of Lethbridge, that derive PWV from the observed atmospheric radiances in the atmospheric band around the 20 μm wavelength (Smith et al. 2001; Riddle et al. 2010, in preparation). The atmospheric water vapor content can be obtained by matching the observed infrared radiances to those computed from a line-by-line, layer-by-layer, radiative transfer model that requires knowledge of the surface pressure, temperature, and the temperature lapse rate, as well as the water vapor scale height. Detailed technical information on the radiometers as well as on the calibration and logic of the line-by-line radiative transfer model is found in Smith (2001) and Naylor et al. (2002).

As an historical note, a prototype IRMA radiometer was developed in the late 1990s by the University of Lethbridge group and tested at the James Clerk Maxwell Telescope (JCMT) site in

Mauna Kea in 1999 December. The motivation for construction of the infrared radiometer and the results of the tests at the JCMT site are given in Smith et al. (2001). This first generation of an IRMA instrument used liquid nitrogen as a reference calibrator. Results of these and of followup tests were encouraging (see, e.g, Fig. 7 in Smith et al. 2001) and were the basis for the decision to use three new-generation IRMA radiometers for the monitoring of water vapor at the TMT candidate sites. Since the prototype IRMA required liquid nitrogen both for cooling the detector and as a calibration source, it required frequent operator support (approximately every few hours) and did not lend itself to a remote deployment. The design of the new generation of IRMA radiometers required significant modifications to allow their autonomous use at remote sites. Major changes included the use of a mechanical Stirling engine to cool the detector to 77 K, and a redesign of the calibration source, which is now attached to the instrument lid.

The three IRMA radiometers were delivered to TMT in 2006 January and a side-by-side comparison campaign was conducted during 3 weeks at Cerro Paranal with the support of the ESO Very Large Telescope staff. This test identified problems with both the hardware and the calibration method, problems that were addressed throughout the next year at the University of Lethbridge. Specifically, the problems found in the calibration of the IRMA instruments were related to temperature gradients in the calibration source and the detection of a stray radiation component traced to reflections within the IRMA enclosure. The net effect of these problems was to introduce bias and variability in the determination of PWV that are due to instrumental issues and do not represent real fluctuations of PWV in the atmospheric column. The latter point was complicated by the fact that, in the absence of a liquid nitrogen reference load, calibration required observations of an ambient blackbody, attached to the inside of the IRMA lid, that could also be heated. Unfortunately, when the blackbody was heated, the thermal environment of the interior of the IRMA enclosure was affected, making calibration of the units more challenging. These problems were eliminated, or reduced, by the addition of temperature sensors at 16 locations across the inside of the IRMA units; cross referencing of the internal calibration load with an external blackbody that contains additional embedded temperature sensors; and the use of an aperture mask in front of the detector. A sophisticated calibration method linking all the different pieces of information was developed in the process (Querel 2007). After these modifications were implemented, the three IRMA units became more stable and they were redeployed for another side-by-side comparison campaign on Cerro Armazones in 2007 January. At that time, the results showed good repeatability between the units, with an output stable at a level of about 0.25 mm over the PWV range from 2 mm to 20 mm that was encountered during the test period. This side-by-side comparison also showed offsets of the order of 0.5 mm between units, which were likely due to remaining uncertainties in the absolute calibration procedure. In common with all remote sensing instruments, the derived PWV values depend on the atmospheric model used and in particular on the physical profiles (e.g., temperature, pressure, composition) of the model, which are site dependent.

The IRMA radiometer concept is currently being redesigned to address the calibration issues identified during the TMT test campaign. The goal is to achieve in future units an absolute calibration accuracy of ± 0.1 mm PWV.

For the interested reader, cryogenics, using liquid helium or liquid nitrogen, for calibration and cooling of sensing instruments operated at remote sites has been shown to be possible. An example of this approach was the use of a Fourier Transform Spectrometer monitoring the atmospheric transmission from 300 GHz to 3.5 THz at the remote area of Chajnantor (Paine et al. 2000).

In summary, the IRMA radiometer installed at the Armazones site produced data that covered about 200 days during 2007 (Fig. 2). As can be seen in Figure 2, there are two large gaps in the time series that affect the last part of the austral summer (February/March) as well as a significant fraction of the austral spring (October/November). The other two IRMA radiometers, which were redeployed to Mauna Kea 13N and Tolonchar after the side-by-side test, were affected by various problems to the point that their scarce data was not of sufficient quality to be used in this study.

3.2 Additional Databases for the Estimation of PWV

In order to gain insight into the magnitude, fluctuations, and statistical properties of PWV at the TMT candidate sites, the IRMA water vapor measurements were supplemented with data sets available from several instruments operated at nearby stations, including surface weather station measurements as well as radiosonde soundings available for cities near the TMT sites. In the case of the sites in northern Chile, the analysis shows that PWV values obtained from radiosonde data for the city of Antofagasta correlate well with the IRMA results (see scatter plot in Fig. 3 for an example). However, a bias between the two data sets is obvious; in § 4 it is shown that this offset, apparent in the scatter plot in Figure 3, can be attributed largely to a dry bias identified in the vertical profiles of humidity measured with radiosondes launched from the city of Antofagasta. In addition, in this study the IRMA PWV data observed at Armazones, after redeployment in 2007, is compared to the PWV inferred from time series of surface water density obtained from measurements of temperature and relative humidity at the site. This comparison (§ 4, Fig. 2) shows good agreement, supporting the use of PWV data estimated from surface measurements as a good way to generate long PWV data series for the statistical analysis of overall and seasonal PWV conditions at all the sites in Chile.

For the case of San Pedro Mártir and the 13N site on Mauna Kea, precipitable water vapor data series were calculated from zenith optical depth data, obtained with a 210 GHz tipping

radiometer and with a 225 GHz tipping radiometer, respectively. Equations (1) and (2) provide the models to convert the optical depths into an equivalent PWV measurement, in mm. The 210 GHz optical depth to PWV model is described in Otárola et al. (2009), while the 225 GHz optical depth to PWV model was communicated to the authors of this study by Simon Radford (2008, private communication):

$$\mathrm{PWV} = 19.46 \times \tau_{0(210\ \mathrm{GHz})} - 0.31, \quad (1)$$

$$\mathrm{PWV} = 21.422 \times \tau_{0(225\ \mathrm{GHz})} - 0.296. \quad (2)$$

The 210 GHz hardware, data acquisition, and calibration at San Pedro Mártir are described in Hiriart et al. (1997) and the 225 GHz radiometer at Mauna Kea is described in the technical reports of Liu (1987) and McKinnon (1987). The use of microwave and millimeter wavelength radiometry for the monitoring of PWV in the atmospheric column is a well-established technique; see, for example, Westwater (1978), Han & Westwater (2000), and Delgado et al. (1999). Additionally, two other important studies in the open literature make use of the 225 GHz radiometers for the conversion of 225 GHz atmospheric radiances into PWV and provide detailed description of the calibration and description of errors affecting this type of measurements: Chamberlain & Bally (1995) and Chamberlain (2004).

4. DATA ANALYSIS

4.1 PWV from IRMA Instrument Observations and Derived from Surface Weather Data

As stated in § 3.2, the IRMA PWV data gathered in 2007 at the Armazones site were compared to results from PWV data series derived from the surface weather data obtained locally at the Armazones site and also from the analysis of atmospheric soundings from a nearby radiosonde station (Antofagasta, 85442 SCFA). Figure 2 shows the comparison of the 2007 IRMA PWV data with those derived from measurements of the surface water vapor density. The latter are computed from surface measurements of temperature and relative humidity obtained with the TMT weather station, and make use of a median value of the water vapor scale height of 1.55 km for data that falls in the summer season and 1.74 km for the data in the rest of the year. These water vapor scale heights were computed from the analysis of profiles of PWV of four years (2004–2007) obtained from vertical atmospheric soundings from the Antofagasta sounding station. The analysis showed that the mean PWV profiles of fall, winter and spring are comparable giving similar

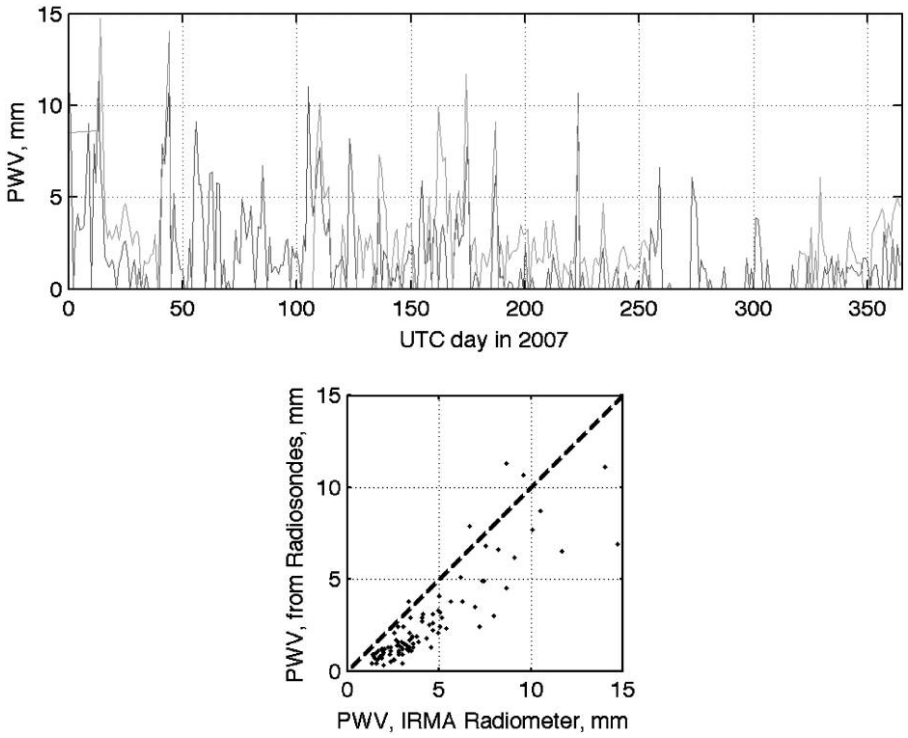

FIG. 3.—Comparison of PWV values obtained with the IRMA radiometer at the Armazones site and the PWV computed from radiosonde soundings available from the Antofagasta sounding station (one sounding a day at 12 UT). (*Top*) the 12 UT time series of IRMA PWV and PWV derived from radiosondes; (*bottom*) the corresponding scatter plot. The identity line in the scatter plot shows the linear correspondence between the IRMA and sounding results, but also demonstrates the offset between the results from the two methods. See the electronic edition of the *PASP* for a color version of this figure.

scale height in the vertical distribution of PWV. The integrated water vapor in the atmospheric column is estimated from the observation of surface weather parameters using the model

$$
\begin{aligned}
e_0 &= e_s \frac{\mathrm{RH}}{100} \qquad e_s = 611.21 \cdot e^{(18.678 - \frac{T(^\circ C)}{234.5})(\frac{T(^\circ C)}{257.14 + T(^\circ C)})} \\
\rho_{V_0} &= \frac{e_0}{R_V \cdot T} \qquad \rho_{V_z} = \rho_{V_0} \cdot e^{-\frac{(z - z_0)}{H}} \\
\mathrm{PWV} &= \int_{z_0}^{z_{\max}} \rho_{V_0} \cdot e^{-\frac{(z - z_0)}{H}} \cdot dz \\
\mathrm{PWV} &= \rho_{V_0} \cdot H \cdot 1000 \cdot (1 - e^{\frac{z_0 - z_{\max}}{H}}).
\end{aligned}
\tag{3}
$$

Here, the variables are: e_0, the surface level partial pressure of water vapor (Pa); e_s, the partial pressure of water vapor (Pa) at saturation as a function of the surface air temperature T (used in degrees Celsius where indicated, otherwise in Kelvin); RH, the surface relative humidity (in percent); ρ_{V_0}, the surface water vapor density (kg m^{-3}); ρ_{V_z}, the water vapor density at the altitude z above sea level (kg m^{-3}) $R_V = 461.9$, the water vapor gas constant (J kg^{-1} K^{-1}); H, the water vapor scale height (km); z_0, the geographic elevation of the site (km); and $z_{\max}$, the maximum altitude in the atmosphere considered for the integration of the water vapor density profile, in this analysis $z_{\max} =$ 12 km. The equation for the determination of the water vapor at saturation is from the Buck Research CR4 Hygrometer Manual (2009).

The time series of precipitable water vapor observed with the IRMA radiometers in 2007 and that estimated from the surface water vapor density, as well as the corresponding scatter plot, are shown in Figure 2. This figure shows two large gaps (the first from mid-February until mid-April and a second one from mid-September until mid-November) when the IRMA radiometer at Armazones did not produce useful data, consequently the available data cover only about 65% of the year. Figure 2 shows no significant difference in the baseline level, and a good match of the baseline-trend throughout the year. Also, the scatter plot computed using daily averages of PWV for the IRMA and surface data PWV shows a reasonably good agreement. However, several very large PWV peaks are seen in the IRMA results that significantly exceed the surface data values. These are likely the result of clouds affecting the IRMA radiometer measurements. It is important to clarify that the determination of the integrated water vapor in the atmospheric column from surface measurements of weather parameters gives accurate results only in the absence of temperature inversion layers aloft, such that water vapor distributes exponentially with altitude with a given scale height. For estimating integrated water vapor in the atmospheric column at Tolar and Armazones from the measurements of surface water vapor density, the water vapor scale heights obtained from the analysis of radiosondes from the Antofagasta stations were used (1.55 km in summer, 1.74 km in all the other seasons). For the case of the higher elevation site of Tolonchar, a scale height of 1.13 km, as reported for the atmosphere above the Chajnantor site (Giovanelli et al. 2001), was used. Similarly, the conversion of atmospheric radiances observed by the IRMA radiometers into an equivalent amount of water vapor in the atmospheric column makes use of a multilayer line-by-line radiative transfer code that has its own water vapor scale height embedded in the model (Chapman et al. 2005). Consequently, an accurate determination is only possible under ideal conditions. A more precise determination of PWV requires knowledge of the vertical distribution of water vapor, e.g., from a radiosonde or nearby weather stations located at different altitudes. If the models used describe average conditions, the average statistics of PWV should be captured correctly by both data sets for the periods for which data are available.

4.2 PWV from Radiosondes Soundings from the Antofagasta Sounding Station

In addition to the IRMA and surface data, a permanent sounding station in the region of Antofagasta within 150 km of Armazones (Antofagasta, 85442 SCFA) launches radiosondes daily at 12:00 UT (9:00 A.M. standard local time, 8:00 A.M. local daylight saving time). The soundings for the period 2004 January 1 through 2007 December 31 were available for this study.[9] The vertical profiles of air temperature and relative humidity were used to compute the vertical profile of water vapor density using the first three steps shown in equation (3). Finally, the integrated water vapor in the atmospheric column is the result of integrating the water vapor density profile from the altitude of the Armazones site up to a cutoff altitude set to 12 km (~204 hPa pressure level). The PWV data series provides a total of 1160 days of coverage during the period from the end of 2004 October, when the surface weather station was installed at Armazones, until the end of 2007 December. Figure 4 shows the cumulative distribution of PWV computed from the soundings and from the PWV data series estimated from the surface weather data. It is very interesting to notice the difference between the statistics obtained from these two methods, with the sounding statistics being drier than those obtained from surface weather station data. A similar offset is also evident in the scatter plot in Figure 3 where the PWV data series of the IRMA radiometer and that derived from the soundings are compared. This discrepancy required some additional research. Considering that the absolute magnitude of the PWV time series from surface data and that from the IRMA radiometer compared reasonably well, we started with the hypothesis that the soundings results were drier than the real behavior of the atmosphere. This implied a dry offset in the determination of the relative humidity. From the statistics in

[9] Soundings downloaded from the Department of Atmospheric Sciences, College of Engineering, University of Wyoming, http://weather.uwyo.edu/upperair/sounding.html.

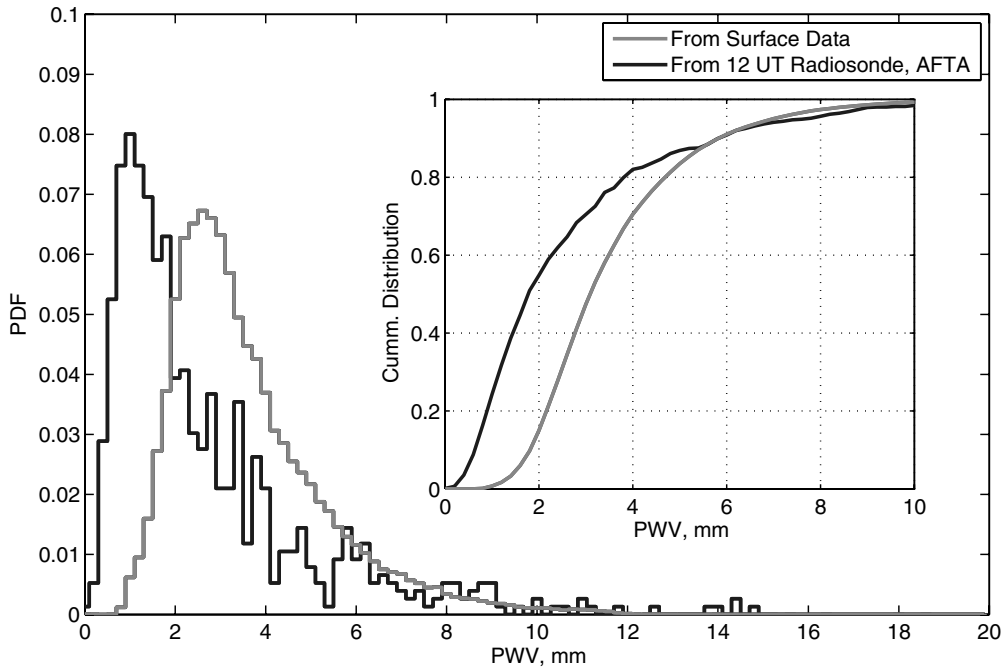

FIG. 4.—Armazones site: normalized histograms and cumulative probability distributions of PWV during the period from 2004 October through 2007 December as estimated from the surface water vapor density (*gray*) and from 12 UT soundings launched from the Antofagasta (85442 SCFA) sounding station (*black*). The water vapor scale heights used to estimate PWV from surface water vapor density are: 1.55 km for summer season data and 1.74 km for all of the other seasons (scale heights were obtained from the analysis of radiosonde profiles).

Figure 4, this offset is estimated to be approximately 1 mm PWV. Making use of a water vapor scale height of 1.74 km, a 1 mm PWV offset translates into a dry bias in the relative humidity sensor of about 7% ($\delta\rho_V \sim 1.0$ Kg/m^2/1800 m $= 5.57E-4$ Kg/m^3, using a mean temperature of 280 K for the site, the relative humidity offset can be estimated from the following expression,$\delta\mathrm{RH} = \delta\rho_V R_V T/e_s(T) \times 100$, with $e_s(T)$ the saturation water vapor pressure at temperature T).

The recent work of Miloshevich et al. (2009) reports on the dry bias that has been identified in the RS92 sounding packages. From Figure 9b in Miloshevich et al. (2009) it is possible to infer that this daytime dry bias goes from about 10% of the measured RH at 700 hPa to about 35% of the measured RH at the 204 hPa pressure level, with a daytime uncertainty, independent of height, of about $\pm 5\%$. The geometric mean of this dry bias is $19\% \pm 5\%$. A quick analysis of the radiosonde profiles from the Antofagasta station indicates the mean RH in the region 700 hPa–204 hPa is about 20%. Therefore, the mean bias expected in the RS92 RH sensor is estimated to be $(19\% \pm 5\%)/100 \times 20\% = (4\% \pm 1\%)$ of RH. The order of magnitude of this RH dry bias is close to that estimated from the offset identify in this study to exist between the PWV derived from the IRMA and radiosonde databases at the Armazones site. This finding, plus the confirmation that the Antofagasta sounding stationhas indeed been using the RS92 sounding model since 2005 April (Aravena, J., 2009, private communication), supports our claim that the PWV time series derived from the radiosonde profiles is most likely affected by a dry bias as observed in Figure 3.

In summary, considering the good agreement of the PWV data series derived from surface water vapor density and the IRMA data series for 2007 found in § 4.1, and illustrated in Figure 2, and the fact that this PWV data series was of sufficient quality to detect the dry biasdry bias in the humidity sensor used in the soundings of the Antofagasta (85442 SCFA) sounding station, we decided to use the surface PWV data as our best estimate of the overall and seasonal statistics of PWV at the three sites in Chile: Tolar, Armazones, and Tolonchar. On the other hand, for the San Pedro Mártir and the Mauna Kea 13N sites, the PWV in the atmospheric column was derived from radiances observed at 210 GHz (see Otárola et al. 2009) and from radiances observed with a 225 GHz radiometer, respectively. In order to provide a further verification that PWV values derived from surface measurements of temperature and relative humidity were good enough to estimate the global statistics of PWV at a given site, this hypothesis was tested for the 13N Mauna Kea site by comparing PWV computed from surface water vapor density to that retrieved from the 225 GHz optical depths by means of equation (2). Daily averages of PWV from both methods and for a total of 680 days are shown in the scatter plot in Figure 5. This scatter plot shows a good agreement, cross-correlation coefficient of 0.8, between the radiometric and surface data methods for deriving PWV at the level of daily averages. This result provides support for using PWV derived from surface measurements

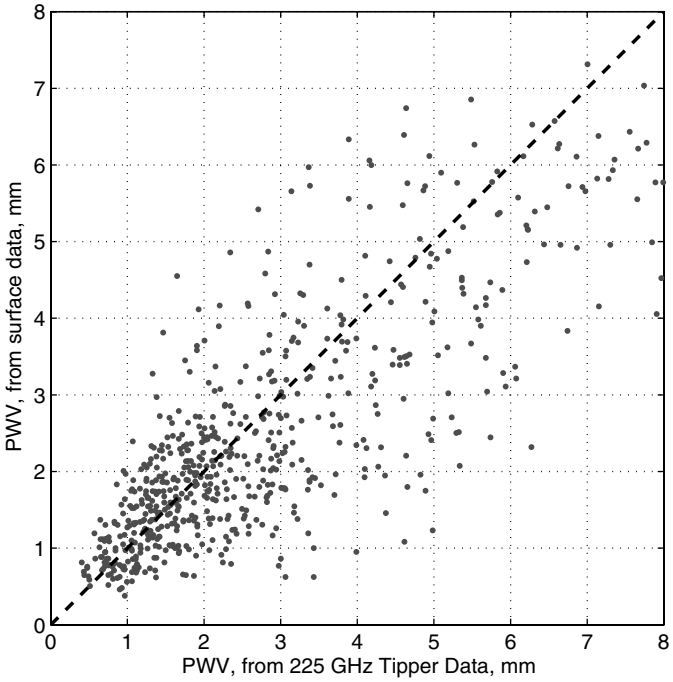

FIG. 5.—Scatter plot using 680 daily averages of PWV estimated from 225 GHz optical depths (using eq. 2 in this article) and from 13N surface water vapor density together with a scale height of 1.1 km at Mauna Kea. The 225 GHz optical depths are observed at the location of the Caltech-Smithsonian Observatory (SAO) site. The cross-correlation coefficient of the 680 daily averages was computed to be 0.8.

of temperature and relative humidity in assessing the global (long-term) statistics of PWV at a given site.

5. RESULTS

5.1 Overall Statistics

Figures 6 and 7 show the overall statistics, in terms of cumulative distribution and histograms, of PWV in the atmospheric column at all TMT candidate sites. The overall median values computed from the available in situ data are included in Table 2 and can be compared to the median values obtained from the preliminary satellite studies by Erasmus & van Staden (2001, 2002, 2003) shown in Table 1. The results from the preliminary studies and those obtained from the in situ site-testing studies are within 30% for all sites. At Armazones, Tolonchar, and Mauna Kea they compare to better than 10% which supports the careful work done by Erasmus and van Staden in the analysis of 6.7 μm GOES satellite images. The surface data for Tolar give a PWV median value of 4.7 mm, about 17% larger than that reported by the Erasmus studies. Considering that Tolar is the lowest elevation site (see Table 1) and that the satellite studies make use of radiances in the 6.7 μm channel whose weighting function is more sensitive to the PWV in the mid- to upper-troposphere (Erasmus & Sarazin 2001; 2002), it is quite possible that in this case the 4.7 mm PWV median value is closer to the actual value for this site. The largest discrepancy was found in the case of San Pedro Mártir,

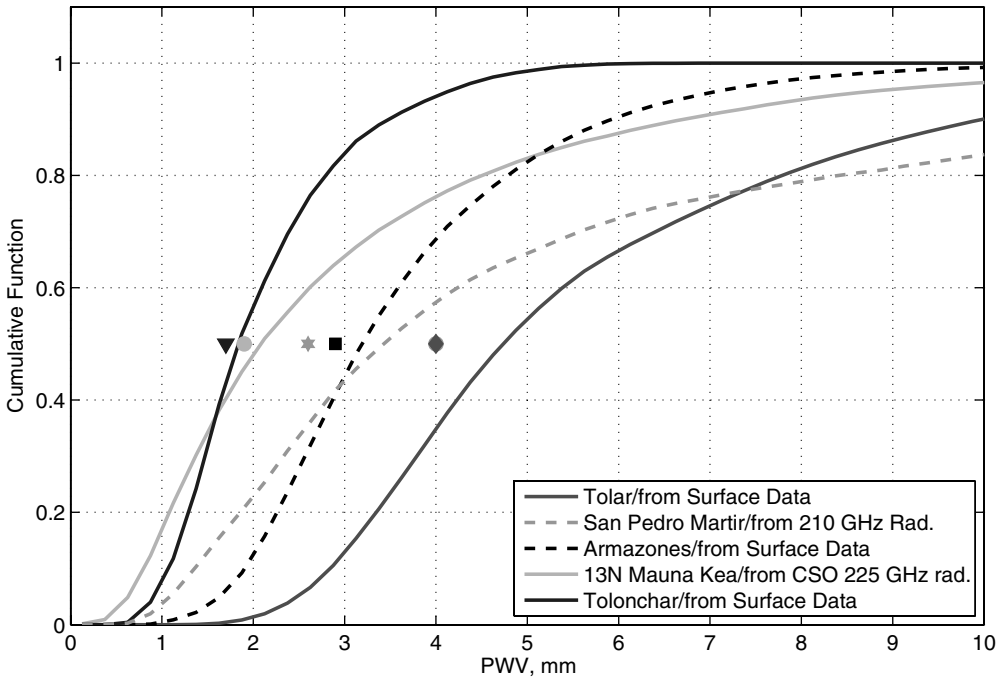

FIG. 6.—Overall statistics: *Solid lines* show the PWV cumulative probability distributions of the TMT candidate sites in the period from late 2004 to the end of 2007. The median values computed for each of the sites from preliminary satellite studies are shown by the following symbols: Tolonchar (*triangle*), 13N Mauna Lea (*circle*), Armazones (*square*), San Pedro Mártir (*star*), Tolar (*diamond*).

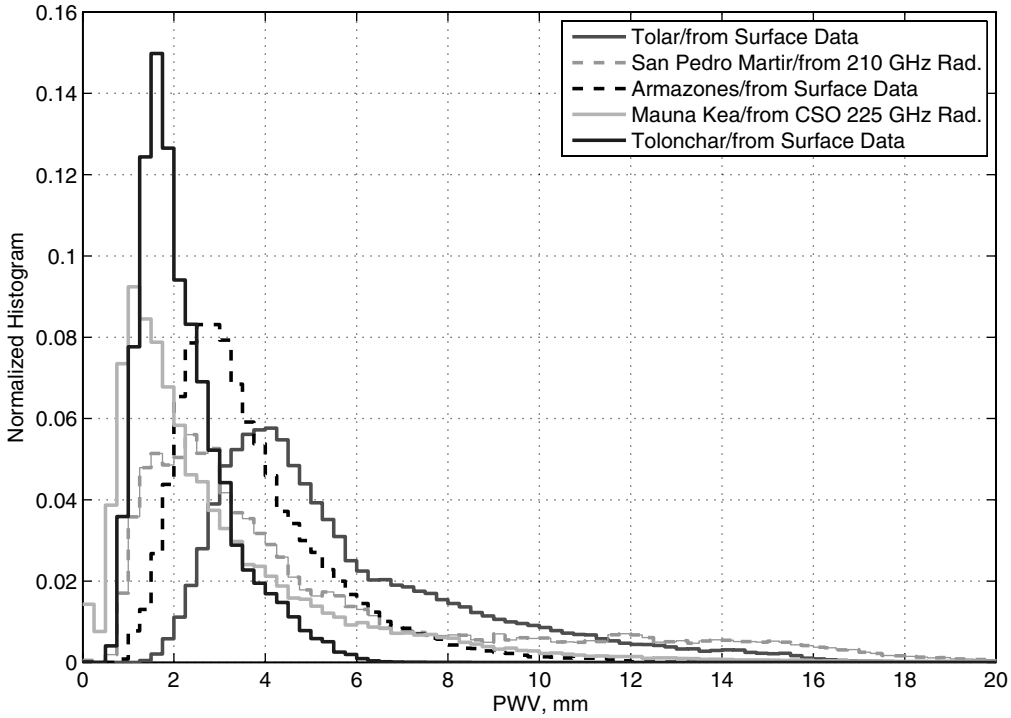

FIG. 7.—Overall statistics: Histograms of PWV of the TMT candidate sites in the period from late 2004 until the end of 2007. Each histogram was normalized to the total number of data points available in each of the corresponding data series.

where the satellite studies give a median value of 2.6 mm while the in situ PWV data series gives a median of 3.4 mm (30% wetter than the preliminary satellite studies). The statistics for San Pedro Mártir came from a data series that included two gaps at the beginning and end of the fall season. If those gaps, falling in a relatively dry season of the year, were filled with the median value of the winter season then the overall median of the San Pedro Mártir site becomes 2.8 mm (Otárola et al. 2009), also within 10% of that anticipated by the Erasmus and van Staden studies.

The histogram shapes in Figure 7 tell something about the differences in climate between the sites as well. For example, while the Tolonchar distribution shows an upper wing that falls quite sharply, an indication of a relatively short and not too variable wet season, the histogram for Tolar shows a longer tail extending to higher PWV values, an indication of a longer wet season. The case of San Pedro Mártir is also special in the sense that its histogram shows a very long tail, extending about 4 standard deviations and with a small secondary peak at about 12 mm of PWV. This confirms the known climate of the site, characterized by a longer and highly variable wet season. However, some of the long tail effect in the histogram might be due to summer clouds illuminating the 210 GHz detection system during the atmospheric scanning.

The overall median PWV values found from the data analysis at the tested sites, plotted in Figure 8, confirm the known paradigm that, on average, the higher a site is, the drier it is. The support for this paradigm lies in the decrease of temperature with altitude and energy considerations that limit the absolute magnitude of water vapor pressure possible at those conditions. However, the Earth's atmosphere is highly unsaturated with respect to water vapor, with an estimated long-term average of about $50\% \pm 5\%$ relative humidity in the latitude band from 60N to 60S and from 200 hPa to 700 hPa along the vertical axis (Cess 2005), and therefore there is plenty of room for natural variability in the PWV between sites at similar geographic altitudes. In fact, one observation from this study is that San Pedro Mártir is drier than Armazones in their respective winter seasons (Table 2) despite the fact that San Pedro Mártir is approximately 200 m lower in elevation than Armazones.

5.2 Seasonal Variability of PWV at the Sites

The PWV data series for each of the TMT candidate sites was split into four different data sets by season, taking into consideration the fact these sites are located in different hemispheres.[10] The first quartile and the median values from the statistical analysis of the seasonal data for each site are shown in Table 2. If attention is given to the seasons when the median PWV is at or below the somewhat arbitrarily chosen value of

[10] Seasons were defined as the following dates (southern hemisphere/northern hemisphere): 03/21-06/20 (fall/spring), 06/21-09/20 (winter/summer), 09/21-12/20 (spring/fall), 12/21-03/20 (summer/winter).

TABLE 2
SUMMARY OF PWV VALUES OBTAINED FROM ANALYSIS OF IN SITU DATA FOR THE TMT CANDIDATE SITES

Season	Tolar 2290 m	San Pedro Mártir 2830 m	Armazones 3064 m	Mauna Kea 4050 m	Tolonchar 4480 m
Summer	5.4/7.5	4.0/7.9	3.8/4.9	1.6/2.4	2.5/3.2
Fall	3.6/4.7	2.3/3.7	2.7/3.5	1.4/2.4	1.5/1.9
Winter	3.1/3.7	1.3/2.2	2.1/2.5	1.0/1.8	1.1/1.3
Spring	3.2/4.0	2.2/3.1	2.1/2.7	1.2/1.8	1.2/1.6
Global results	3.6/4.7	2.1/3.4	2.4/3.2	1.2/2.1	1.4/1.8

NOTE.—First quartile values (in mm), format: 25% to left of /, median, to right. Results are shown by season and overall data set available for each site from early 2004 through the end of 2007. The exception is San Pedro Mártir, whose statistics are based only on the 210 GHz radiances observed in 2006 (see text and Otárola et al. 2009 for details).

3.1 mm, we see that the San Pedro Mártir and the Armazones sites are quite comparable, with both sites characterized by dry winter and spring seasons. The Tolonchar median PWV values are below 2.0 mm for the fall, winter, and spring seasons, and the summer statistics almost made the cut of the 3.1 mm set in this example. In the case of Mauna Kea, the statistics show that the median values are below 3.1 mm for all seasons. While the Tolonchar statistics for fall, winter, and spring are slightly better than those for Mauna Kea, the main difference is seen in the summer season when Tolonchar is affected by the moist air advected to the region due to the change in the regional circulation, from the southward shift and weakening of the high-pressure system off the coast of northern Chile (Fuenzalida et al. 1987; Zhou & Lau 1998).

The seasonal histograms and cumulative distributions of PWV are shown in Figure 9. They show many of the same effects pointed out before, such as the dry conditions of San Pedro Mártir in the winter and spring season and the highly variable and wet atmospheric conditions during the summer season indicated by the long tail of the histogram that includes a clear secondary peak at 12 mm of PWV. Another important characteristic is the large number of occurrences of low PWV values at the Tolonchar site for the fall, winter, and spring seasons, while Mauna Kea is drier than Tolonchar during the summer season.

In addition to the "the higher, the drier" paradigm, the data shown in Figure 9 and Table 2 also confirm another rule of thumb, that winter is the driest season at all five locations tested by TMT, closely followed by the spring season.

6. MID- AND FAR-INFRARED CAPABILITIES OF THE TMT TESTED SITES

As stated in § 1, the relevance of researching the magnitude and variability of the concentration of water vapor in the atmospheric column for the location of astronomical facilities has to do with minimizing the atmospheric thermal background that affects the performance of mid-infrared detection systems and limits the use of the mid-infrared and far-infrared bands as potential windows for astronomical research. Consequently, a low water vapor content in the atmospheric column makes the atmosphere more transparent, and opens opportunities for astronomers to research objects of astronomical interest, at bands that carry important information for understanding the physical and dynamic processes taking place in these objects. Examples of these processes are included in the TMT Detailed Science Case (Silva et al. 2007 and references therein). One such example is the physics of star formation, where mid-IR observations can help detect stars that are heavily obscured by dense molecular clouds; other examples include: star-forming cores and their accretion disks, where mid-IR and far-IR emission can help elucidate the total luminosity of the forming star and its accretion disk; determination of the timescale for the dissipation of gas in circumstellar objects using molecular and atomic tracers in environments, where given the temperature magnitude, the emission of the spectral lines falls between 1 and 25 μm, and with the relevance that this dissipation timescale is strongly associated with the viability of the formation of giant planets; the detection of prebiotic molecules with spectral lines lying in the mid-IR band (Knez et al. 2005); research on molecular species in the atmospheres of exoplanets (Burrows et al. 2004) as well as in the atmospheres of solar system objects (Roe et al. 2003).

For completeness, the modeled atmospheric transmissions expected for the TMT candidate sites have been included in this article (Fig. 10). The calculations were done for the best PWV quartile (Fig. 10a) and the median PWV conditions (Fig. 10b) obtained for these sites from the analysis of the PWV data series and shown in Table 2. The atmospheric transmission for the best quartile and mean conditions was computed using a multilayer, line-by-line near-IR to far-IR radiative transfer model (NIRFIR_RTM[11]) that uses the HITRAN 2008 molecular spectroscopic database (Rothman et al. 2009), which includes the contributions to the atmospheric absorption by H_2O, CO_2, O_3, N_2O, CO, CH_4, and O_2 molecules without considering the effect of their isotopic species.

The science drivers and design overview of a TMT mid-infrared echelle spectrograph (Elias et al. 2006) state that the instrument performance is relatively insensitive to PWV in the range from 8 μm to 13 μm, while for longer wavelengths, water vapor is critical. Consequently, the transmission plots

[11] The NIRFIR_RTM atmospheric transmission model was implemented by A. Otárola on a MATLAB ® platform.

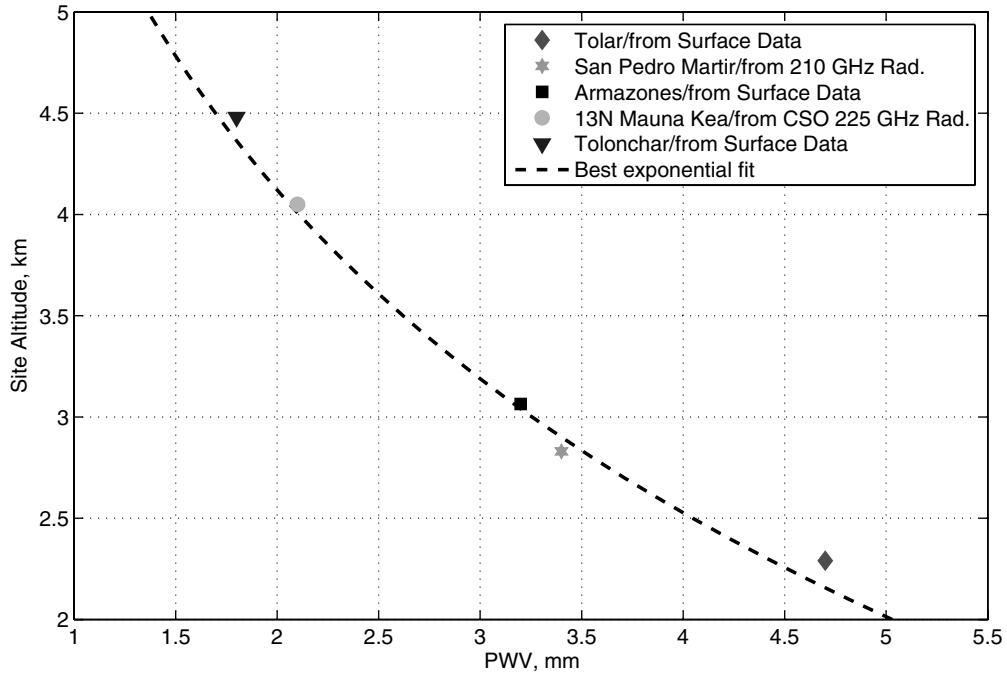

FIG. 8.—Overall median PWV values obtained in this study for the five TMT candidate sites in the period from 2004 until the end of 2007. The dashed line represents the exponential function that best fit the median PWV values and is given by the equation $\mathrm{PWV}(z) = 12 \cdot e^{-\frac{z(\mathrm{km})}{2.3\,\mathrm{km}}}$ with results in mm. Symbols are defined in Fig. 6.

shown in this study emphasize the wavelength range from 17 μm to 28 μm that lies right after the wide atmospheric CO_2 absorption band centered at about 15 μm.

The transmission plots show that in the best PWV statistical quartile (winter season), Tolonchar and Mauna Kea are the best of all sites considered in this study and have similar atmospheric transmission levels. In both cases, the transmission in the most affected atmospheric window (considered in this study) between 27 μm and 28 μm reaches 70%.

Figure 10b shows that for the overall median PWV conditions there is a larger difference between Tolonchar (55% transmission) and Mauna Kea (48% transmission), with Tolonchar having approximately 15% better transmission in the 27 μm to 28 μm window. For reference, we note that under the median PWV conditions at the summit of Chajnantor, an exceptionally dry site, the sky transmission in the 27 μm to 28 μm window reaches almost 90% (see Fig. 2 in Sako et al. 2008).

The overall median PWV shows that the atmospheric transmissions at San Pedro Mártir and Armazones are more comparable in magnitude. However, in the relative comparison of the sites, attention should also be paid to the fact, as shown in the seasonal PWV histograms in Figure 9, that the summer season at San Pedro Mártir is wetter and more prolonged that in Armazones.

7. INTERPRETATIONS AND CONCLUSIONS

The Thirty Meter Telescope project conducted a site-testing campaign at five sites that were preselected based on satellite infrared image studies (Erasmus & van Staden 2001; 2002; 2003). These sites exhibit overall median values ranging from 1.8 mm PWV for the highest site to 4.7 mm for the lowest site. The overall relative comparison of the five sites is well illustrated by Figure 8, which shows the median values as a function of the site altitude, and confirms the paradigm that the higher the site is, the drier it is. An exponential model that represents the best fit to the median PWV reported in Figure 8 is presented in equation (4), in which PWV is given in mm as a function of altitude, z, above mean sea level in km

$$\mathrm{PWV}(z) = 12 \times e^{-\frac{z}{2.3}}. \quad (4)$$

All the sites tested by TMT are located in geographic areas that are naturally dry. In the case of the Atacama Desert, the dryness is explained by the high altitude of the Andes mountain range and its mechanical influence on the zonal mean flow that is deflected northward, producing the South Pacific subtropical anticyclone with subsidence of dry air (Rodwell & Hoskins 2001; Takahashi et al. 2007). At Mauna Kea, the dryness is explained by a combination of main direction of the air flow, orographic precipitation, advection of dry air and geographical altitude, while San Pedro Mártir's dryness is explained by the location of the semipermanent high-pressure system in the east Pacific.

Concerning humidity trends, recent studies using the NCEP reanalysis data series for the period 1973–2007 show indications of a negative humidity trend above 700 hPa in the tropical regions, on the order of 1% every 10 years (Fig. 4 in Paltridge et al. 2009). This negative trend in humidity lies below the

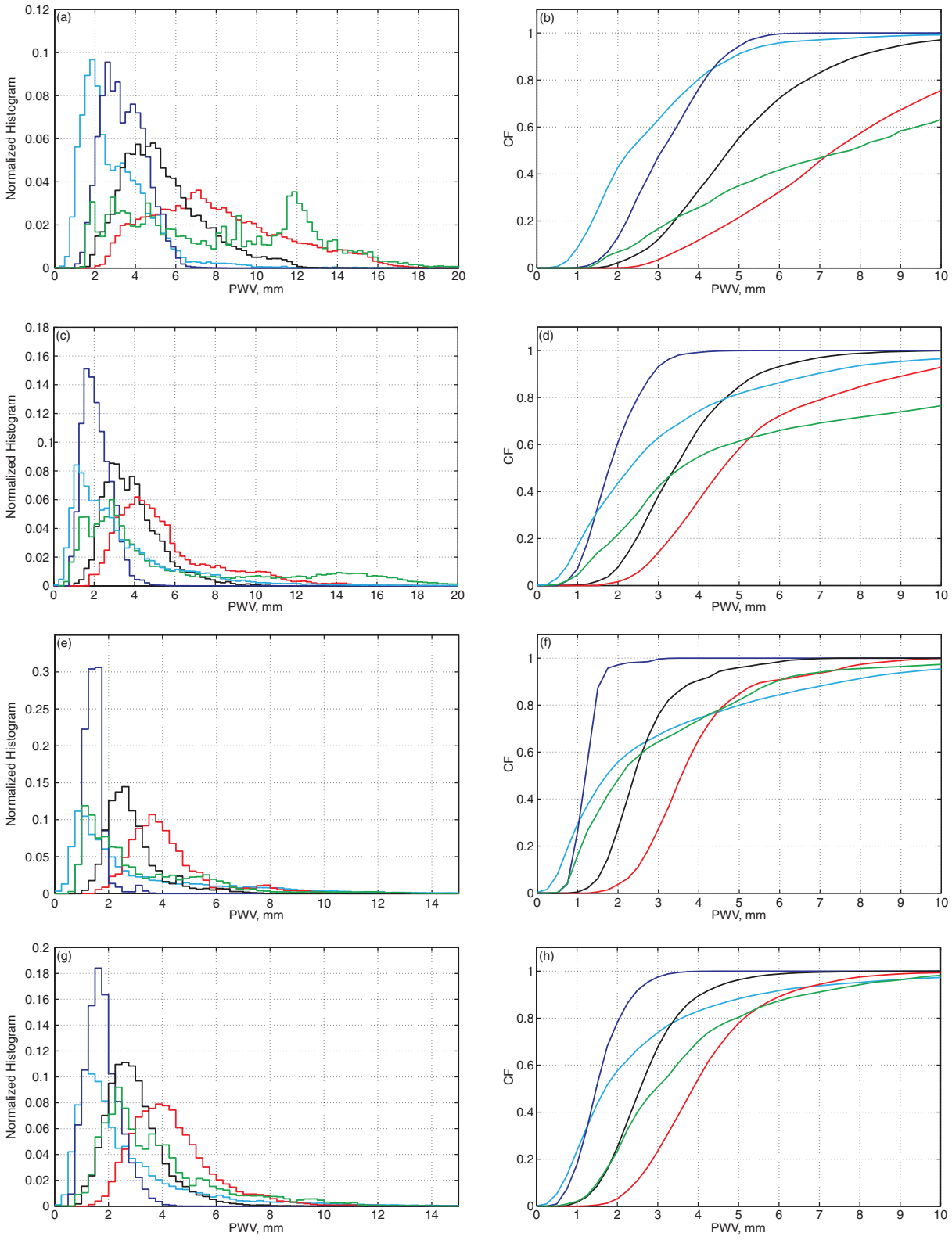

FIG. 9.—Seasonal statistics for (*a,b*) summer, (*c,d*) fall, (*e,f*) winter, (*g,h*) spring: Histograms of PWV of the TMT candidate sites in the period from late 2004 until the end of 2007. Each histogram was normalized to the total number of data points available in each of the corresponding data series. Sites are identified by color: *red*, Tolar; *green*, San Pedro Mártir; *black*, Armazones; *cyan*, Mauna Kea; *blue*, Tolonchar.

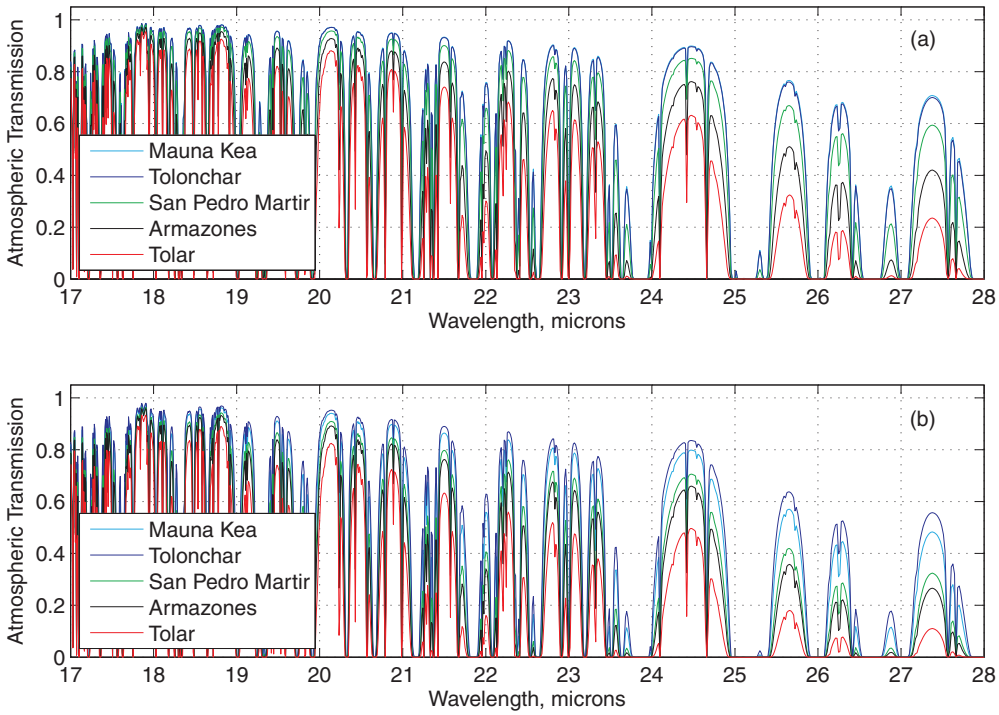

FIG. 10.—Atmospheric transmission at the five sites tested by TMT in the wavelength region from 17 to 28 μm for (*a*) the best quartile PWV values, and (*b*) the overall median PWV values. The transmission spectra makes use of the averages of the winter and annual vertical pressure and temperature profiles computed for each site from the nearest permanent radiosonde station (Antofagasta, San Diego, and Hilo, respectively). The water vapor density profiles were normalized such that the integrated PWV profile amounts to (*a*) the best quartile PWV values, and (*b*) the overall median PWV values, respectively.

accuracy of standard humidity sensors. The analysis of Otárola et al. (2005, Fig. 16) of PWV estimated from measurements of surface water vapor density in the region of Antofagasta, and for the period 1973–2004, does not show an obvious trend, but it does show the dryness of the site and the humid signature of atmospheric oscillations such as El Niño. The feedback in the PWV as a function of an increase in the mean temperature of the planet, based strictly on energy considerations, is expected to be positive. This implies an increase in atmospheric water vapor as the result of an increase in the mean temperature of the planet. However, this increase is only explained in the sense of global averages. Dessler et al. (2008), from the analysis of height-resolved specific humidity and relative humidity in the period 2003–2008 using NASA's AIRS data, show that over most of the troposphere, specific humidity has increased as a result of the increasing global average surface temperature, but that some regions, including the tropics, show the opposite. Thus, no statements about the expected long-term changes in precipitable water vapor can be made for the TMT candidate sites.

The seasonal statistics of PWV at the five sites shows that all sites are particularly dry during their respective winter and spring seasons with PWV median values below 3.1 mm for all sites except Tolar, the lowest elevation site, and below 2 mm in the case of Mauna Kea and Tolonchar, the highest elevation and driest of the five sites. The very low PWV content in the atmospheric column at sites like Mauna Kea and Tolonchar is favorable for observation in the mid-IR, and into the far-IR bands, as shown by the transmission spectra in Figure 10.

We thank David Hiriart and Simon Radford for their valuable contributions and for allowing us access to their 210 GHz and 225 GHz tipping radiometers databases, respectively, and Greg Tompkins for providing technical support for IRMA. The authors also thank an anonymous reviewer for valuable comments and suggestions that helped improve this manuscript. We thank Andrea Ferrara for important grammar suggestions that helped improve the readability of this manuscript. The TMT Project gratefully acknowledges the support of the TMT partner institutions. They are the Association of Canadian Universities for Research in Astronomy (ACURA), the California Institute of Technology, and the University of California. This work was supported as well by the Betty Moore Foundation, the Canada Foundation for Innovation, the Ontario Ministry of Research and Innovation, the National Research Council of Canada, the Natural Sciences and Engineering Research Council of Canada, the British Columbia Knowledge Development Fund, the Association of Universities for Research in Astronomy (AURA), and the US National Science Foundation.

REFERENCES

Adams, D. K., & Comrie, A. C. 1997, BAMS, 78, 2197

Aumann, H. H., Chahine, M. T., Gautier, C., Goldberg, M. D., Kalnay, E., McMillin, L. M., Revercomb, H., Rosenkranz, P. W., Smith, W. L., Staelin, D. H., Strow, L. L., & Susskind, J. 2003, IEEE Trans. Geo. Rem. Sens., 41, 253

Buck Research Instruments, L.L.C. 2009, CR4 Hygrometer Manual, hygrometers.com/wp-content/uploads/CR-4-users-manual-ver-2.pdf

Burrows, A., Surdarsky, D., & Hubeny, I. 2004, ApJ, 609, 407

Cess, R. D. 2005, Science, 310, 795

Chamberlain, R. A., & Bally, J. 1995, JIMW, 16, 907

Chamberlain, M. A., Ashley, M. C. B., Burton, M. G., Phillips, A., Storey, J. W. V., & Harper, D. A. 2000, AJ, 535, 501

Chamberlain, R. A. 2001, J. Geo. Res., 106, 20101

Chamberlain, R. A. 2004, Pub. Astron. Soc. Austr., 21, 264

Chapman, I. M., & Naylor, D. A. 2005, Development of a Freely Distributed, Customizable Atmospheric Radiative Transfer Model, in Fourier Transform Spectroscopy/ Hyperspectral Imaging and Sounding of the Environment, Technical Digest (CD) (Optical Society of America), paper HTuD2

Delgado, G., Otárola, A., Belitsky, V., Urbain, D., Hills, R., & Martin-Cocher, P. 1999, ALMA Memo 271.1, http://www.alma.nrao.edu/memos/

Dessler, A. E., Zhang, Z., & Yang, P. 2008, Geoph. Res. Lett., 35, L20704

Elias, J. H., Carr, J. S., Richter, M. J., Najita, J., Chun, M. R., Tokunaga, A. T., Liu, M., Lacy, J., Strom, S., Liang, M., & Bond, T. W. 2006, Proc. SPIE, 6269, 62693

Erasmus, D. A. 2005, Proc. IAU Symp. 232, ed. Whitelock, P., Dennefeld, M., & Leibundgut, B., 510

Erasmus, D. A., & Sarazin, M. 2001, Proc. SPIE, 4168, 317

Erasmus, D. A., & Sarazin, M. 2002, ASP Conf. Ser. 266, ed. Vernin, J., Benkhaldoun, Z., & Muñoz-Tuñon, C. 310

Erasmus, D., & van Staden, C. 2001, A Satellite Survey of Water Vapor and Cloud Cover in Northern Chile, Final Report, Cerro-Tololo Inter-American Observatory

Erasmus, D., & van Staden, C. 2002, A Satellite Survey of Cloud Cover and Water Vapor In The Southwestern U.S.A. and Northern Mexico, Final Report, California Extremely Large Telescope

Erasmus, D., & van Staden, C. 2003, A Comparison of Satellite-Observed Cloud Cover and Water Vapor At Mauna Kea and Selected Sites In Northern Chile, The Southwestern U.S.A. and Northern Mexico, Final Report, AURA New Initiatives Office

Fuenzalida, H., & Ruttlant, J. 1987, in Proc. II Congreso Interamericano de Meteorologia, Buenos Aires, 6.3.1

Giovanelli, R., Darling, J., Henderson, C., Hoffman, W., Barry, D., Cordes, J., Eikenberry, S., Gull, G., Keller, L., Smith, J. D., & Stacey, G. 2001, PASP, 113, 803

Han, Y., & Westwater, E. R. 2000, IEEE Trans. Geosci. Remote Sensing, 38, 1260

Hiriart, D., Goldsmith, P., Skrutskie, F., & Salas, L. 1997, Rev. Mex. AA, 33, 59

Knez, C., et al. 2005, ApJ, 635, 145

Kursinski, E. R., Bennett, R. A., Gochis, D., Gutman, S. I., Holub, K. L., Mstaler, R., Minjarez, C., Minjarez, I., & van Hove, T. 2008, Geo. Res. Lett., 35, L03815

Lau, K.-M., & Li, M.-T. 1984, BAMS, 65, 114

Liu, Z.-Y. 1987, NRAO Internal Report #271

Maddox, R., McCollum, D., & Howard, K. 1995, Weather Forecasting, 10, 763

McKinnon, M. 1987, NRAO Memo #40

Minier, V., Olmi, L., Lagage, P.-O., Spinoglio, L., Durand, G. A., Daddi, E., Galilei, D., Gallée, H., Kramer, C., Marrone, D., Pantin, E., Sabbatini, L., Schneider, N., Tothill, N., Valenziano, L., & Veyssière, C. 2008, EAS Publ. Ser., 33, 21

Miloshevich, L., Vömel, H., Whiteman, D., & Leblanc, T. 2009, J Geophys. Res., 114, D11305

Naylor, D. A., Gom, B. G., Schofield, I. S., Tompkins, G. J., & Chapman, I. M. 2002, Proc. SPIE, 4820, 908

Paltridge, G., Arking, B., & Pook, M. 2009, Theoretical and Applied Climatology, DOI: 10.1007/s00704-009-0117-x

Otárola, A., Delgado, G., Booth, R., Belitsky, V., Urbain, D., Radford, S., Hofstadt, D., Nyman, L., Shaver, P., & Hills, R. 1998, ESO Messenger, 94, 13

Otárola, A., Hiriart, D., & Pérez-León, J. E. 2009, Rev. Mex. AA, 45, 161

Otárola, A., Holdaway, M., Nyman, L-Å., Radford, S. E. J., & Butler, B. 2005, ALMA Memo # 512. Available from http://www.alma.nrao.edu/memos/

Paine, S., Blundell, R., Cosmo Papa, D., Barrett, J. W., & Radford, S. 2000, PASP, 112, 108

Querel, R. R. 2007, M.S. thesis, Univ. Lethbridge, Alberta, Canada

Randel, D. L., Vonder Haar, H., Ringerud, M. A., Stephens, G. L., Greenwald, T. J., & Combs, C. L. 1996, BAMS, 77, 1233

Rodwell, M. J., & Hoskins, B. J. 2001, J. Climate, 14, 3192

Roe, H. G., Greathouse, T. K., Ritcher, M. J., & Lacy, J. H. 2003, AJ, 597, L65

Rothman,et al. 2009, J. Quant. Spectroscopy Radiative Transfer, 110, 533

Sako, S.,et al. 2008, Proc. SPIE, 7012, 70122

Sarazin, M. 2005, Proc. IAU Symp. 232, ed. Whitelock, P., Dennefeld, M., & Leibundgut, B., 34

Schöck, M., Els, S., Riddle, R. L., Skidmore, W., Travouillon, T., Blum, R., Bustos, E., Chanan, G., Djorgovski, G., Gillett, P., Gregory, B., Nelson, J., Otárola, A., A., Seguel, J., Vasquez, J., Walker, A., Walker, D., & Wang, L. 2009, PASP, 121, 384

Silva, D., Hickson, P., Steidel, C., & Bolte, M. 2007, TMT Detailed Science Case

Simpson, J. J., Berg, J. S., Koblinsky, C. J., Hufford, G. L., & Beckley, B. 2001, Rem. Sens. Env., 76, 112

Smith, G. J. 2001, M.S. thesis, Univ. Lethbridge, Alberta, Canada

Smith, G. J., Naylor, D. A., & Feldman, P. A. 2001, Int. J. Infr. Mill. Wav., 22, 661

Takahashi, K., & Battisti, D. S. 2007, J. Climate, 20, 3434

Walker, A. 2002, ASP Conf. Ser. 266, in Vernin, J., Benkhaldoun, Z., & Muñoz-Tuñon, C., 466

Wallace, J. M., & Hobbs, P. V. 2006, Atmospheric Science: An Introductory Survey (2nd ed., New York: Academic Press-Elsevier)

Westwater, E. R. 1978, IEEE Trans. Geosci. Remote Sensing, 13, 677

Zhou, J., & Lau, K.-M. 1998, J. Clim., 11, 1020